Supplementary Information for "Computational spectropolarimetry with a tunable liquid crystal metasurface"

Yibo Ni, Chen Chen, Shun Wen, Xinyuan Xue, Liqun Sun, Yuanmu Yang*

State Key Laboratory of Precision Measurement Technology and Instruments, Department of Precision Instrument, Tsinghua University, Beijing 100084, China

**Corresponding author:* ymyang@tsinghua.edu.cn

1 Design methodology of the liquid crystal metasurface

We initiate the tunable metasurface as one-dimensional silicon grating embedded in liquid crystal, which is further covered with a transparent indium-tin-oxide (ITO) electrode. With such a configuration, the fabrication of the liquid crystal metasurface is compatible with the mature complementary metal-oxide semiconductor (CMOS) and liquid crystal on silicon (LCoS) manufacturing process.

The thickness of the silicon grating is fixed at 500 nm, since it is known that a photonic crystal slab with a thickness of ~λ_0/n can support multiple guided-mode resonances around a central wavelength λ_0, where n is the refractive index of the material [1]. The shape of the nanostructure is fixed as a one-dimensional grating for simplicity, as a one-dimensional grating is known to exhibit large anisotropy. Other shapes, such as cut-wires, can also be used at the cost of a larger design space. The thickness of the liquid crystal layer is chosen as 2.5 μm to minimize the cell gap so as to ensure a relatively fast switching speed for the liquid crystal. With the abovementioned geometric parameters, the only remaining tuning knobs of the metasurface are the period and width of the grating. We, therefore, performed an exhaustive sweep of the two parameters and obtained a library of the Mueller matrix $\mathbf{M}_0^{\theta}(\lambda)$ at each λ and θ_{LC}. For each pair of geometric parameters, we calculated correlation coefficient matrices $\mathbf{C}_{00}$, $\mathbf{C}_{01}$, $\mathbf{C}_{02}$ and $\mathbf{C}_{03}$ of the Mueller matrix over the target wavelength range. The figure-of-merit (FoM) to choose the period and width of the grating is then defined as the summation of the norm of each correlation coefficient matrix $\mathrm{FoM} = \sum_{i=0}^{3} \left\| \mathbf{C}_{0i} \right\|_1$, where $\left\| \mathbf{C}_{0i} \right\|_1$ is the L^1 norm of $\mathbf{C}_{0i}$.

At the current stage, we certainly have not exhausted options to further enhance the anisotropy or Q-factors of the guided-mode resonances in order to achieve better device performance. Although not within the scope of the current work, one may optimize the device performance by introducing freeform nanostructures. The metasurface containing freeform nanostructures may be optimized efficiently via inverse-design methods such as the adjoint method [2].

2 Derivation of the Mueller matrix

Since the Jones calculus is a concise and adequate way to describe completely polarized light, and any Jones matrix can be transformed into the corresponding Mueller matrix, we first sort to use the Jones matrix to describe the liquid crystal metasurface.

The Jones matrix of the measurement system $\mathbf{J}$ is given by,

$$\mathbf{J} = \mathbf{J}_{\mathrm{p}} \cdot \mathbf{J}_{\mathrm{meta}} \tag{S1}$$

where $\mathbf{J}_{\mathrm{p}}$ and $\mathbf{J}_{\mathrm{meta}}$ are Jones matrices of the polarizer and liquid crystal metasurface, respectively. The Jones matrix of the polarizer whose transmission axis is at an angle

θ_{p} from the x-axis (as defined in Fig. 2a of the main text) is given by,

$$\mathbf{J}_{\mathrm{p}} = \begin{bmatrix} \cos\theta_p & -\sin\theta_p \\ \sin\theta_p & \cos\theta_p \end{bmatrix} \begin{bmatrix} 1 & 0 \\ 0 & 0 \end{bmatrix} \begin{bmatrix} \cos\theta_p & \sin\theta_p \\ -\sin\theta_p & \cos\theta_p \end{bmatrix} = \begin{bmatrix} \cos^2\theta_p & \cos\theta_p \sin\theta_p \\ \cos\theta_p \sin\theta_p & \sin^2\theta_p \end{bmatrix} \quad \text{(S2)}$$

The liquid crystal metasurface, with its director lying in the yz-plane, does not possess chirality. $\mathbf{J}_{\mathrm{meta}}$ is diagonal with the form,

$$\mathbf{J}_{\mathrm{meta}} = \begin{bmatrix} r_x & 0 \\ 0 & r_y \end{bmatrix} \quad \text{(S3)}$$

where r_{x} and r_{y} represent the complex amplitude reflection of x- and y-polarized light, respectively. Thus,

$$\mathbf{J} = \mathbf{J}_{\mathrm{p}} \cdot \mathbf{J}_{\mathrm{meta}} = \begin{bmatrix} \cos^2\theta_p & \cos\theta_p \sin\theta_p \\ \cos\theta_p \sin\theta_p & \sin^2\theta_p \end{bmatrix} \begin{bmatrix} r_x & 0 \\ 0 & r_y \end{bmatrix} = \begin{bmatrix} r_x \cos^2\theta_p & \cos\theta_p \sin\theta_p \\ r_x \cos\theta_p \sin\theta_p & r_y \sin^2\theta_p \end{bmatrix} \text{(S4)}$$

The Jones matrix $\mathbf{J}$ can be transformed into the Mueller matrix following the relation [3],

$$\mathbf{M} = \mathbf{A}(\mathbf{J} \otimes \mathbf{J}^*)\mathbf{A}^{-1} \quad \text{(S5)}$$

where * represents the complex conjugate,

$$\mathbf{A} = \begin{bmatrix} 1 & 0 & 0 & 1 \\ 1 & 0 & 0 & -1 \\ 0 & 1 & 1 & 0 \\ 0 & i & -i & 0 \end{bmatrix} \quad \text{(S6)}$$

and $\otimes$ is the tensor (Kronecker) product.

By substituting Eq. (S4) into Eq. (S5), the first row of the Mueller matrix of the measurement system M_0 can be obtained as,

$$M_0 = \frac{1}{2} \begin{bmatrix} |r_{\mathrm{x}}|^2 \cos^2\theta_{\mathrm{p}} + |r_{\mathrm{y}}|^2 \sin^2\theta_{\mathrm{p}} \\ |r_{\mathrm{x}}|^2 \cos^2\theta_{\mathrm{p}} - |r_{\mathrm{y}}|^2 \sin^2\theta_{\mathrm{p}} \\ |r_{\mathrm{x}}||r_{\mathrm{y}}| \sin(2\theta_{\mathrm{p}}) \cos(\Delta\varphi) \\ |r_{\mathrm{x}}||r_{\mathrm{y}}| \sin(2\theta_{\mathrm{p}}) \sin(\Delta\varphi) \end{bmatrix}^{\mathrm{T}} \quad \text{(S7)}$$

where $\Delta\varphi = \arg(r_{\mathrm{x}}) - \arg(r_{\mathrm{y}})$.

3 Calculation of correlation coefficients

To ensure the fidelity of the spectropolarimetric measurement, each column of the measurement matrix $\mathbf{M}_0^{\theta}(\lambda)$ at each λ and θ_{LC}, denoted as $M_{0l}^{\theta}(\lambda)$, needs to be designed to have a minimal correlation. $M_{0l}^{\theta}(\lambda)$ is an $N \times 1$ vector with the form $M_{0l}^{\theta}(\lambda) = \left[m_{0l}(\lambda, \theta_{\mathrm{LC}}^{1}) \quad m_{0l}(\lambda, \theta_{\mathrm{LC}}^{2}) \quad \dots \quad m_{0l}(\lambda, \theta_{\mathrm{LC}}^{N}) \right]^{\mathrm{T}}$, where N is the total number of measurements and θ_{LC}^{i} is the i^{th} value of θ_{LC}. l represents the column number in the Mueller matrix, $l = 0, 1, 2, 3$.

We define the correlation coefficient as [4],

$$c_{0l}(\lambda_i, \lambda_j) = \frac{\mathrm{cov}(M_{0l}^{\theta}(\lambda_i), M_{0l}^{\theta}(\lambda_j))}{\sigma_{\boldsymbol{M}_{0l}^{\theta}(\lambda_i)} \sigma_{\boldsymbol{M}_{0l}^{\theta}(\lambda_j)}} \tag{S8}$$

where $c_{0l}(\lambda_i, \lambda_j)$ is the correlation coefficient between $M_{0l}^{\theta}(\lambda_i)$ and $M_{0l}^{\theta}(\lambda_j)$. cov and σ represent the covariance operation and the standard deviation, respectively.

According to the simulated complex amplitude reflection of the metasurface, we calculate correlation coefficients over the wavelength range from 1300 nm to 1600 nm. As shown in Fig. S1, the calculated correlation coefficients of the Mueller matrix are relatively small over the wavelength range from 1400 nm to 1500 nm, suggesting good spectral diversity required for high-fidelity spectral reconstruction.

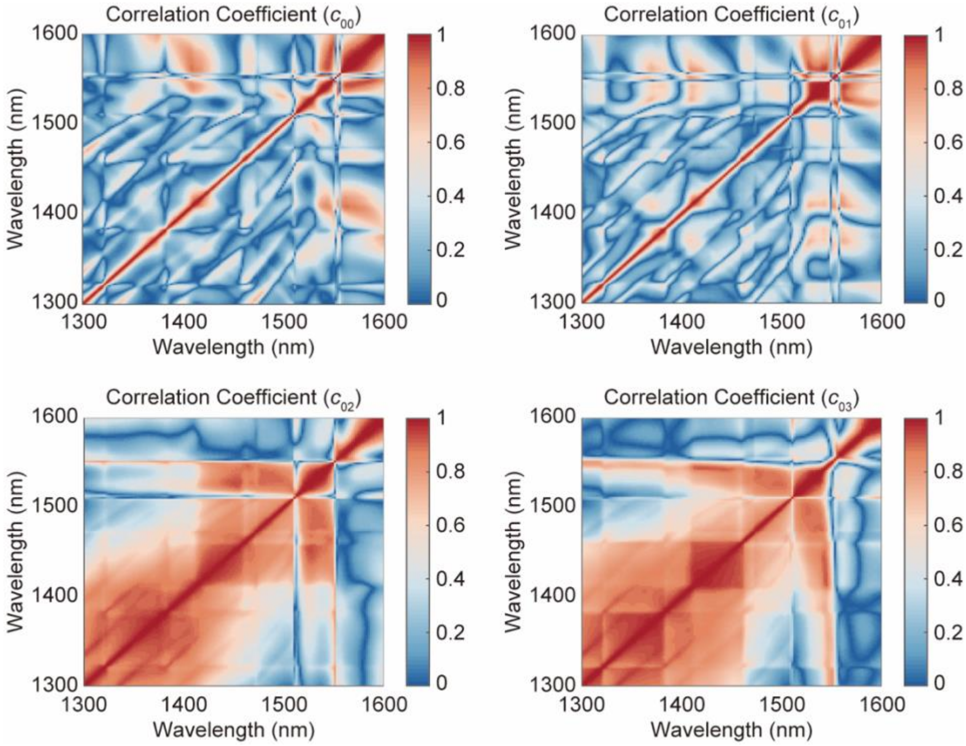

Figure S1 Calculated correlation coefficients of the Mueller matrix c_{00}, c_{01}, c_{02}, and c_{03} over the wavelength range from 1300 nm to 1600 nm.

4 Sample fabrication

The sample fabrication was performed via a commercial service (Tianjin H-Chip Technology Group) and started with a silicon-on-insulator (SOI) wafer with a device layer thickness of 500 nm and a buried thermal oxide layer thickness of 2 μm as the substrate. The resistivity of silicon is about 10 Ω•cm. The silicon grating was patterned by the standard electron-beam lithography process using PMMA as the resist. After the resist development process, a 30 nm Chromium (Cr) layer was deposited by electron beam deposition. Through a lift-off process, the pattern was transferred to the Cr film. Subsequently, the SOI sample was etched by reactive ion etching using the Cr film as a hard mask. In the final step, the Cr mask was removed using wet etching.

A commercial ITO conductive glass is used as the top covering substrate to form the liquid crystal cell. A layer of sulphuric azo-dye (SD1) was first spin-coated on both the SOI and ITO substrate, followed by curing at 100 °C for 10 minutes on a hot plate. A layer of glue mixed with silica microspheres with a uniform diameter of 2.5 μm was then dripped on the SOI substrate. Subsequently, the ITO substrate was pressed onto the SOI substrate with the gap length defined by the diameter of the silica microsphere. The glue layer was cured by ultra-violet (UV) light irradiation. The liquid crystal cell was then irradiated by a linearly polarized UV light for 15 minutes, such that the SD1 layer became a liquid crystal alignment layer with the anchoring direction along the polarization direction. Lastly, nematic E7 liquid crystal molecules were infiltrated into the cell by the capillary force and aligned to the desired direction.

5 Experimental setup

The experimental setup for both the Mueller matrix calibration and spectropolarimetric measurement is schematically illustrated in Fig. 4a in the main text. The light source is a supercontinuum laser (YSL Photonics, SC-Pro-7) that was first routed through a monochromator (Zolix, Omni-λ2007i). The monochromatic light with a spectral bandwidth of about 1.5 nm is then output through a single-mode fiber and a collimation lens. The collimated light sequentially passes through a polarizer (P1) and a λ/4 waveplate (WP) so that the polarization state can be arbitrarily modulated. The incident light is then focused by a lens with a focal length of 100 mm to reduce the beam diameter to about 100 μm while maintaining the angle of incidence within ± 0.5°.

The reflected light from the metasurface passes through a broadband non-polarizing beam splitter (BS) and a polarizer (P2), whose transmission axis is at an angle θ_p from the x-axis. The modulated light is collected by a lens and measured by a photodetector (Thorlabs, DET10C2). To align the position of the incident beam and the metasurface, we illuminate the metasurface with a white light source (Thorlabs, SLS201L/M) and set up a 4-f system to image the metasurface onto an InGaAs camera (Hamamatsu C14041-10U).

6 Experimentally measured reflectance

The reflectance of the liquid crystal metasurface is measured with the above-mentioned experimental setup. We set the incident light to be polarized along the x-axis and sweep the voltage applied to the metasurface in the range from 0 V to 10 V, and the corresponding reflectance spectra are shown in Fig. S2. Without the applied voltage, the main guided-mode resonance peak has a central wavelength of 1446 nm, which agrees well with the simulation. However, the trend of reflectance change as a function of the applied voltage does not agree quite well with the assumption of a uniform change of the liquid crystal orientation angle.

Several factors may contribute to the problem. On the one hand, to ensure uniform liquid crystal orientation in the static case, we use a liquid crystal alignment layer with strong anchoring energy. However, the strong anchoring also makes it difficult for liquid crystal molecules near substrates to be oriented along the applied electric field, making the refractive index distribution non-uniform. On the other hand, the silicon subwavelength grating has a small resistivity of about 10 Ω•m, which affects the electric field distribution between the SOI and ITO substrate and further disturbs the orientation of liquid crystal molecules. These issues may be overcome by reducing the alignment layer thickness, using liquid crystal with smaller twist elastic constant [5] and replacing the doped silicon with non-conductive silicon.

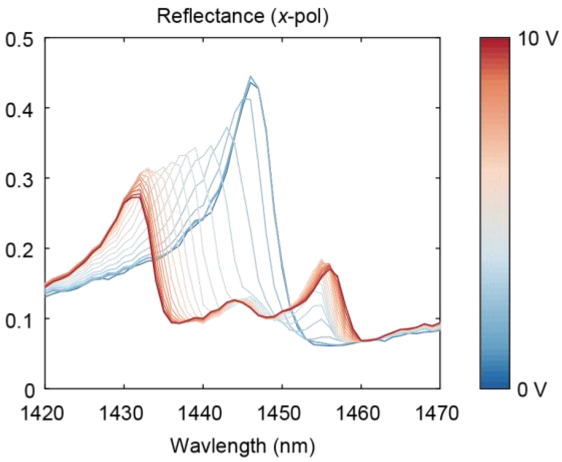

Figure S2 The experimentally measured reflectance for incident light polarized along the *x*-axis as a function of the voltage applied to the metasurface.

7 Condition number of the measurement matrix

The spectropolarimetric measurement process can be mathematically represented as solving a matrix inversion problem, which follows a simplified version of Eq. (2) in the main text,

$$S_{\mathrm{out},0}^{V} = \mathbf{M}_0^V \cdot S_{\mathrm{in}} \tag{S9}$$

in which the condition number κ of the measurement matrix $\mathbf{M}_0^V$ can be used to evaluate the robustness of the solution S_{in} against a given noise in the measured $S_{\mathrm{out},0}^{V}$ [6]. κ is defined as $\kappa = \|\mathbf{M}_0^{V^{-1}}\| \cdot \|\mathbf{M}_0^V\|$, where $\|\mathbf{M}_0^V\|$ is the L^2 norm of $\mathbf{M}_0^V$ and $\mathbf{M}_0^{V^{-1}}$ is the inverse matrix of $\mathbf{M}_0^V$. If κ is large, even a small error in $S_{\mathrm{out},0}^{V}$ may cause a large error in the solution S_{in}. With the existing metasurface design, the coefficient matrix $\mathbf{M}_0^V$ can be adjusted by changing θ_p according to Eq. (3) in the main text. The calculated κ within the wavelength measurement range from 1420 nm to 1470 nm as a function of θ_p is shown in Fig. S3. θ_p is chosen as 45° to minimize the condition number κ around the targeted wavelength range.

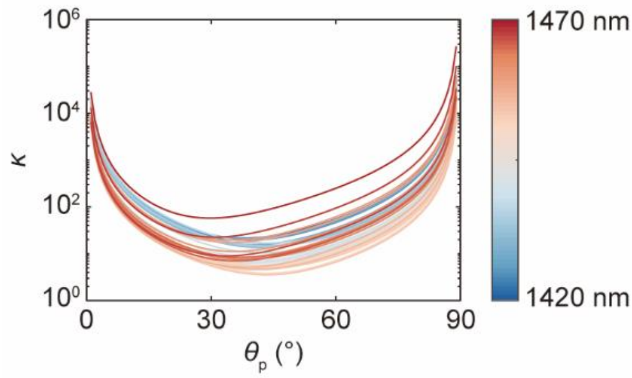

Figure S3 Calculated condition number κ of the measurement matrix $\mathbf{M}_0^V$ as a function of θ_p.

8 Spectropolarimetric reconstruction of dual-peak spectra

Based on the experimentally measured Mueller matrix $\mathbf{M}_0^V(\lambda)$, we numerically reconstructed an unknown input light source with a dual-peak spectrum, assuming an FWHM of 10 nm for each peak and a spectral separation of 12 nm and 20 nm, respectively. The reconstructed polarization and spectrum are compared with the ground truth, as shown in Fig. S4a and S4b, respectively. Despite the decent polarization reconstruction accuracy, we observe that one can reconstruct the spectral peak location with a resolution in the 10-20 nm range. The spectral reconstruction accuracy gradually deteriorates as the peak approaches each other. The relatively low resolution is due to the relatively strong correlation in the measured Mueller matrix.

The fidelity of spectral reconstruction can be greatly improved with a lower correlation of the Mueller matrix. To illustrate the point, we performed additional dual-peak reconstruction using the simulated Mueller matrix with a lower correlation. Here, we assumed an unknown input light source with a dual-peak spectrum with an FWHM of 2 nm for each peak and a spectral separation of 3 nm to 5 nm, respectively. The reconstruction results, as illustrated in Figs. S4c-e, show that one could distinguish dual-spectral peaks with high fidelity with a resolution down to 3 nm.

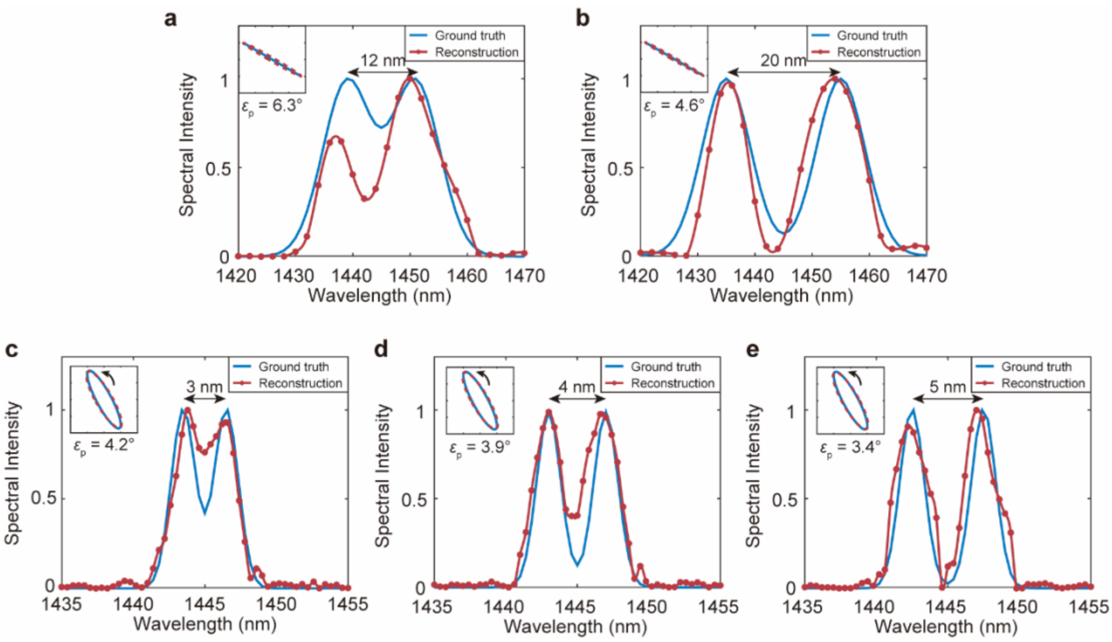

Fig. S4 Spectropolarimetric reconstruction results of dual-peak spectra. **a,b** Reconstructed dual-peak spectra with a fixed FWHM of 10 nm for each peak and a spectral separation of 12 nm (**a**) and 20 nm (**b**), respectively, based on the experimentally measured Mueller matrix. Dashed and solid lines in insets represent reconstructed polarization states and the ground truth, respectively. **c-e** Reconstructed dual-peak spectra with a fixed FWHM of 2 nm for each peak and a spectral separation of 3 nm (**c**), 4 nm (**d**), and 5 nm (**e**), respectively. Dashed and solid lines in insets represent reconstructed polarization states and the ground truth, respectively, based on the simulated Mueller matrix.

9 Transmissive metasurface design

To realize an even more compact spectropolarimetry system, we also designed a transmissive liquid crystal metasurface consisting of a one-dimensional subwavelength grating patterned on a silicon-on-sapphire substrate, as shown in Fig. S5a. In such a way, the metasurface may be directly integrated with a focal plane array camera. The transmissive liquid crystal metasurface is also designed to support multiple guided mode resonances. Here, the ITO cover glass and doped silicon layer can serve as the top and bottom electrodes, respectively. When a voltage is applied to the metasurface, the resonance wavelengths of the metasurface shift following the reorientation of the liquid crystal. The simulated transmittance as a function of the rotation angle of liquid crystal for incident light polarized along the x- and the y-axis is shown in Fig. S5b and Fig. S5c, respectively.

We further numerically tested broadband spectropolarimetric reconstruction with the designed transmissive metasurface, using a broadband left-elliptically polarized incident light source, as shown in Fig. S5d. Similar to the case of the reflective liquid crystal metasurface, the polarization reconstruction result agrees very well with the ground truth, while the spectrum reconstruction error is higher due to the finite spectral correlation of the measurement matrix. An elliptically polarized narrowband with a spectral peak position ranging from 1450 nm to 1550 nm and a bandwidth of 2 nm is reconstructed to verify the spectral resolution. A few representative reconstruction results are shown in Fig. S5e.

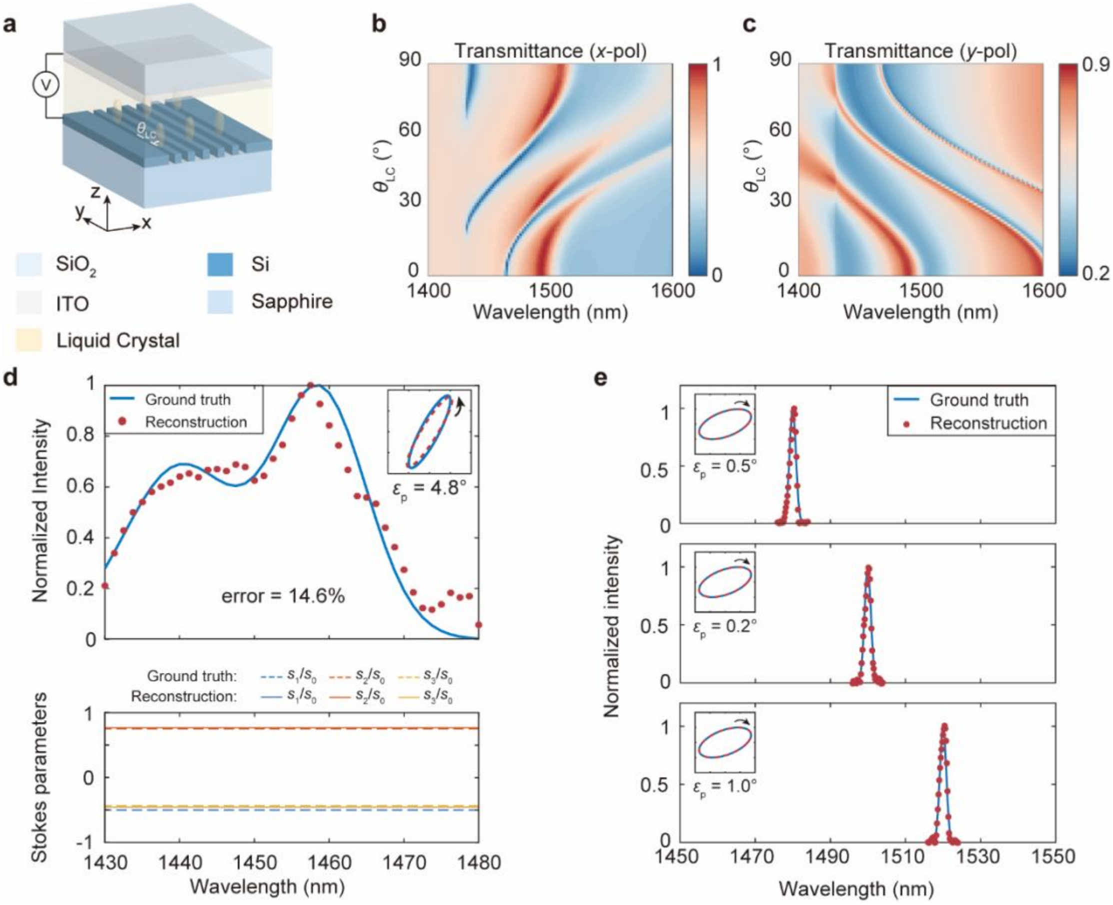

Figure S5 Transmissive liquid crystal metasurface design with numerical spectropolarimetric reconstruction results. **a** Schematic of the transmissive liquid crystal metasurface with voltage applied. **b,c** Simulated transmittance for incident light polarized along the *x*-axis (**b**) and *y*-axis (**c**), respectively. **d** Comparison between numerically reconstructed broadband spectra (represented by dots) and the ground truth (represented by solid lines), respectively. Dashed and solid lines in the inset represent reconstructed polarization states and ground truth, respectively. **e** Reconstructed narrowband spectra with a fixed bandwidth of 2 nm and peak positions of 1480 nm, 1500 nm, and 1520 nm, respectively. Dashed and solid lines in insets represent reconstructed polarization states and the ground truth, respectively.

10 Spectropolarimetric imaging system design

A transmissive liquid crystal metasurface may be well suited for spectropolarimetric imaging since it does not perturb the wavefront of the incident light. For a spectropolarimetric imaging system, we envision a transmissive liquid crystal metasurface directly integrated with the imaging sensor, as illustrated in Fig. S6. Other than the compact form factor, an additional advantage of this approach is that to realize spectropolarimetric imaging with many pixels, one only needs to apply a uniform voltage across the entire array of liquid crystal metasurface.

One of the challenges to realizing this proposal is that it requires the metasurface's aperture size to be large enough to match the size of the image sensor, which is typically in the centimeter range. However, despite the fact that a large-area metasurface is difficult to fabricate using electron-beam lithography, The fabrication of the liquid crystal metasurface is fully compatible with the mature CMOS and LCoS manufacturing process, such that the system may be extended to a much larger scale in the future.

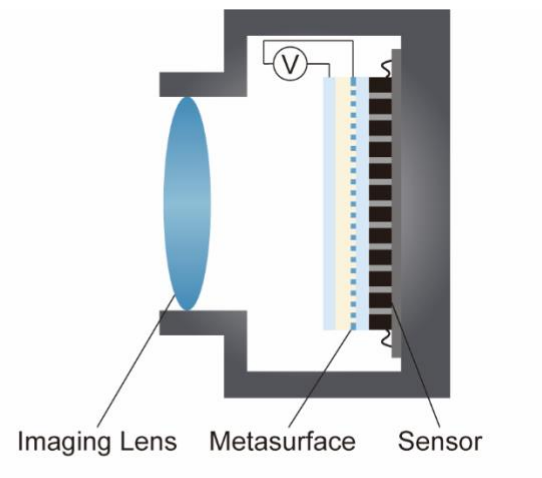

Figure S6 Possible schematic of a liquid crystal metasurface-based spectropolarimetric imaging system.

11 Repeatability of the liquid crystal metasurface's response

The repeatability of the liquid crystal metasurface's response is key for practical applications. In our experiment, we used a widely-adopted type of liquid crystal, E7, and followed the standard liquid crystal cell assembly process, which can help improve the robustness of the device. To verify the device's repeatability, we measured the voltage-dependent reflectance of the liquid crystal metasurface for different wavelengths and polarization states, with each set of data averaged over 100 cycles. The mean measured reflectance, denoted as $\overline{R}$, and the corresponding error bars that show the upper and lower limit of the error are shown in Fig. S7. The maximum relative deviation from the mean value $\overline{R}$ is 15%. Such a deviation in the measured reflectance corresponds to a maximum *SNR* of 8 dB for the measurement system. From the analysis in Figs. 3c,d in the main text, with a maximum *SNR* of 8 dB in the measured reflectance, the metasurface-based spectropolarimeter can still reconstruct the polarization state and wavelength of monochromatic light with high fidelity ($\varepsilon_p < 5°$ and $\varepsilon_\lambda < 0.5\%$).

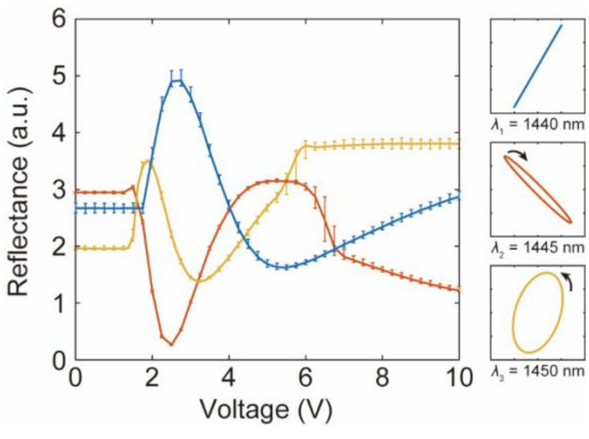

Figure S7 Measured voltage-dependent reflectance of the liquid crystal metasurface. Different colors correspond to different wavelengths and polarization states of the incident light, as shown on the right. The solid lines are the mean measured reflectance $\bar{R}$ over different operation cycles. The error bars mark the upper and lower limit of the error in the measured reflectance.

Reference

1 S.S. Wang, R. Magnusson. Theory and applications of guided-mode resonance filters. Applied Optics **32**, 2606-2613, (1993)

2 S. Molesky, Z. Lin, A.Y. Piggott, W. Jin, J. Vucković, A.W. Rodriguez. Inverse design in nanophotonics. Nature Photonics **12**, 659-670, (2018)

3 A.A. Kokhanovsky. Light scattering reviews 4: single light scattering and radiative transfer (Springer Science & Business Media, 2009).

4 J. Lee Rodgers, W.A. Nicewander. Thirteen Ways to Look at the Correlation Coefficient. The American Statistician **42**, 59-66, (1988)

5 Y. Geng, L. Yao, V. Chigrinov, H.S. Kwok. Analysis of the rewriting time of liquid crystal optical rewritable e-paper. Liquid Crystals **41**, 610-614, (2014)

6 D.A. Belsley, E. Kuh, R.E. Welsch. Regression diagnostics: Identifying influential data and sources of collinearity (John Wiley & Sons, 2005).